Nuclear Engineering and Technology 54 (2022) 627–636

Contents lists available at ScienceDirect

Nuclear Engineering and Technology

journal homepage: www.elsevier.com/locate/net

Original article

The effect of UV-C irradiation and EDTA on the uptake of Co^{2+} by antimony oxide in the presence and absence of competing cations Ca^{2+} and Ni^{2+}

Leena Malinen [a], Eveliina Repo [b], Risto Harjula [a, 1], Nina Huittinen [c, *]

[a] Department of Chemistry, Radiochemistry Unit, University of Helsinki, A. I. Virtasen Aukio 1 (P.O. Box 55), 00014, Finland
[b] Department of Separation Science, School of Engineering Science, LUT University, Yliopistonkatu 34, 53850, Lappeenranta, Finland
[c] Helmholtz-Zentrum Dresden - Rossendorf, Institute of Resource Ecology, Bautzner Landstraße 400, 01328, Dresden, Germany

ARTICLE INFO

Article history:
Received 19 June 2021
Accepted 2 August 2021
Available online 3 August 2021

Keywords:
Cobalt
EDTA
Sorption
Antimony oxide
UV-C
Competing cations

ABSTRACT

In nuclear power plants and other nuclear facilities the removal of cobalt from radioactive liquid waste is needed to reduce the radioactivity concentration in effluents. In liquid wastes containing strong organic complexing agents such as EDTA cobalt removal can be problematic due to the high stability of the Co-EDTA complex. In this study, the removal of cobalt from $NaNO_3$ solutions using antimony oxide (Sb_2O_3) synthesized from potassium hexahydroxoantimonate was investigated in the absence and presence of EDTA. The uptake studies on the ion exchange material were conducted both in the dark (absence of UV-light) and under UV-C irradiation. Ca^{2+} or Ni^{2+} were included in the experiments as competing cations to test the selectivity of the ion exchanger. Results show that UV-C irradiation noticeably enhances the cobalt sorption efficiency on the antimony oxide. It was shown that nickel decreased the sorption of cobalt to a higher extent than calcium. Finally, the sorption data collected for Co^{2+} on antimony oxide was modeled using six different isotherm models. The Sips model was found to be the most suitable model to describe the sorption process. The Dubinin-Radushkevich model was further used to calculate the adsorption energy, which was found to be 6.2 kJ mol^{-1}.

1. Introduction

Solidification and volume reduction of liquid radioactive waste produced by nuclear power plants (NPPs) and other nuclear facilities is required to decrease aqueous radioactivity emissions and to obtain suitable waste forms for final disposal. One of the most problematic waste nuclides found in the liquid waste is ^{60}Co, a corrosion product with a relatively long half-life (5.2 a) and high gamma decay energy (1332 keV and 1173 keV) [1]. ^{60}Co forms stable chelates with ethylenediaminetetraacetic acid (EDTA) which is an aminopolycarboxylic acid complexing agent used in the decontamination processes in nuclear facilities.

Even though the use of EDTA in the nuclear industry has been reduced, EDTA-containing liquid wastes from power plants generated in earlier years can be found stored in tanks. For example, Samuels et al. [2] reported that the 149 radioactive waste tanks at the Hanford Complex in the US contain 83 tons of EDTA. The removal of ^{60}Co in the presence of EDTA is problematic due to the stability of the complexes. EDTA forms water-soluble 1:1 complexes with di- and trivalent metal ions, coordinating the metal ion by forming several heteroatomic rings around the metal center [3]. Straightforward complex formation with tetravalent germanium, tin, titanium, zirconium, hafnium and thorium in acidic solution was reported by Langer [4].

Compared to other metal-ligand complexes, the ring formation leads to a higher stability of the complexes. EDTA is resistant to biodegradation and very heat resistant, implying that formed metal-chelates are very stable and difficult to destroy. However, a promising elimination process using photodegradation has been demonstrated for e.g. Fe(III)-EDTA complexes under environmental

* Corresponding author.
E-mail address: n.huittinen@hzdr.de (N. Huittinen).
[1] Died September 11, 2017.

https://doi.org/10.1016/j.net.2021.08.002

conditions. Here, Kari and Giger [5] showed that Fe(III) can be photodegraded rapidly in shallow rivers. Metsärinne et al. [6] compared the photodegradation of the Na and Fe(III) complexes of EDTA in distilled and in lake water at pH 3.1 and 6.5. They reported that EDTA can be photodegraded only as Fe(III)-EDTA complex and that the photodegradation is pH dependent, being much faster when the original pH of the solution was 3.1 rather than 6.5. According to Lockhart and Blakeley [7] the main photodegradation products of Fe(III)-EDTA are carbon dioxide, formaldehyde, iminodiacetic acid (IMDA), *N*-aminoethyleneglycine (EDMA), *N*,*N*′-ethylenediglycine (EDDA-N,N′), *N*-carboxymethyl-*N*-aminoethylen eglycine (EDDA-N,N), *N*-carboxymethyl-*N*,*N*′-ethylenediglycine (ED3A) and glycine. They studied the photodegradation of Fe(III)-EDTA at three different pH values (pH 4.5, 6.9 and 8.5) and reported that the degradation rate of Fe(III)-EDTA was fastest at pH 4.5.

Few studies have been published on the destruction of the Co^{2+}-EDTA complex. For example, CoTreat® has been tested for the removal of cobalt from EDTA-bearing solutions through sorption on the ion exchange material [8]. The experiments were conducted using UV oxidation in the presence and absence of a photocatalyst, TiO_2, and other oxidants such as H_2O_2 and methods such as ozonation. It was reported that oxidation of EDTA was required for efficient removal of cobalt, and ozonation was found to be the most suitable oxidation method. One of the latest publications on cobalt decomplexation from EDTA has been written by Rekab et al. [9]. They reported that UV oxidation of the complex with the addition of H_2O_2 resulted in a higher rate of organic mineralization than UV oxidation with TiO_2. When TiO_2 was used for the adsorption of cobalt after the oxidation of the Co-EDTA complex by UV-light and H_2O_2, higher decontamination factors were achieved in comparison to the simultaneous use of TiO_2 as a photocatalyst and adsorbent.

The removal of ^{60}Co from nuclear waste effluents after a potential decomplexation from EDTA using various sorbent materials can be hampered by the presence of other cations present in the waste effluent. The liquid waste often contains only trace amounts of radionuclides and high concentrations of stable metal ions, which may be retained to some extent even by highly selective ion exchange materials. It has been reported that the activity concentration of ^{60}Co in a floor drain water at the Loviisa nuclear power plant (Finland) is 402 Bq L^{-1} [10]. This would correspond to a concentration of $1.6 \cdot 10^{-13}$ mol L^{-1}. The concentrations of various stable ions or compounds are comparatively high: $1.6 \cdot 10^{-3}$ mol L^{-1} Na^+, $0.20 \cdot 10^{-3}$ mol L^{-1} K^+, $0.021 \cdot 10^{-3}$ mol L^{-1} Ca^{2+} and $2.6 \cdot 10^{-3}$ mol L^{-1} H_3BO_3 [10]. These macro-elements, especially the divalent cation Ca^{2+}, may influence the removal of cobalt from solution. In addition, other chemically similar divalent transition metals present in much lower concentrations in the waste solutions may compete for the sorption sites on the solid material.

In the present study, we have studied the removal of trace amounts of cobalt from aqueous solution in the absence and presence of EDTA as complexing agent and Ca^{2+} and Ni^{2+} as competing metal cations. Ni^{2+} is released into the aqueous phase by the corrosion of the nuclear reactor vessel and Zircaloy cladding material surrounding the nuclear fuel rods. As a sorbent material, we have chosen the ion exchange material antimony oxide (Sb_2O_3). This study builds on previously published work, where we investigated the use of antimony oxide for the removal of cobalt from 0.01 mol L^{-1} $NaNO_3$ solutions containing EDTA [11]. In that paper, high cobalt sorption efficiencies up to 99.7 % were attained under UV-C irradiation with the antimony oxide synthesized from antimony pentachloride. Due to the corrosiveness of antimony pentachloride, this study reports on the synthesis of antimony oxide using potassium hexahydroxoantimonate, which is a less harmful chemical and therefore more suitable for larger scale production.

The uptake studies on the new ion exchange material were conducted both in the dark (absence of UV-light) and under UV-C irradiation, to account for the potential photodegradation of the Co-EDTA complexes and subsequent Co removal from solution by the antimony oxide. The selectivity of the material for Co^{2+} was tested in the presence of Ca^{2+} or Ni^{2+}. Finally, the retention of Co^{2+} on the ion exchanger was modeled with various isotherm models to describe the sorption process.

2. Experimental

2.1. Materials

Analytical grade $KSb(OH)_6$ (Sigma Aldrich), $Co(NO_3)_2 \cdot 6H_2O$ (Riedel de Haën), $Na_2EDTA \cdot 2H_2O$ (Merck), $Ca(NO_3)_2 \cdot 4H_2O$ (Sigma Aldrich), $Ni(NO_3)_2 \cdot 6H_2O$ (Merck), HCl (VWR), NH_3 (Merck), NaOH (Riedel de Haën), HNO_3 (Fisher Scientific) and chemically pure $NaNO_3$ (VWR, GPR® Rectapur®) were used without further purification. The radioactive tracer, carrier free ^{57}Co, was obtained from Eckert & Ziegler Isotope products. Water from a Milli-Q water purification system (18 MΩ cm) was used for the preparation of solutions.

2.2. Synthesis of the antimony oxide

Synthesis of antimony oxide was performed by modifying the synthesis presented by Khan and Alam [12]. Instead of keeping the reaction mixture at room temperature overnight, 0.1 mol of $KSb(OH)_6$ and 1 L 5.8 mol L^{-1} HCl were mixed using magnetic stirring and heated to 60 °C. Mixing was continued for 30 min to dissolve $KSb(OH)_6$ in the acid. Ammonia (25 %) was added. To keep the synthesis temperature below 70 °C the addition was done slowly, over a duration of 20 min. In the synthesis presented by Khan and Alam [12], ammonia was added until a residual acidity of 0.75 mol L^{-1} HCl was obtained. In the present study ammonia was added until the reaction mixture pH rose to 2.0. The white antimony oxide precipitate was washed several times with water and dried at room temperature.

2.3. Characterization of the antimony oxide

The identification of the crystal phase of the synthesized antimony oxide was determined by powder X-ray diffraction (XRD) using a Panalytical X'pert Pro MDP X-ray diffraction system and X'pert High Score Plus software. The zeta potential of the synthesized antimony oxide was measured with a Malvern Zetasizer Nano ZS which uses Laser Doppler Micro electrophoresis and patented M3-PALS (Phase Analysis Light Scattering) to measure the zeta potential. The solid material and 0.01 mol L^{-1} $NaNO_3$ solution (pH adjusted with 0.1 mol L^{-1} HNO_3 or 0.1 mol L^{-1} NaOH as necessary) were equilibrated for four days using constant rotary mixing (50 rpm) before filtering the sample solution with a 10 μm Acrodisc PSF filter (PALL Life Sciences). The Malvern Zetasizer Nano ZS is designed to measure 5 nm to 10 μm particles, thus it was decided to use the 10 μm filtering as sample pretreatment. The surface morphology of the material was analyzed using a Hitachi S-4800 field emission scanning electron microscope (FE-SEM). BET surface area and total pore volume of the studied material was determined by nitrogen adsorption at 77 K using Autosorb-1-C surface area and pore size analyzer (Quantachrome, The UK).

2.4. Experimental procedure

Prior to the experiments, 0.01 mol L^{-1} $NaNO_3$ test solutions with varying amounts of other chemicals were prepared and traced with

^{57}Co, the tracer activity being <35 kBq L^{-1} corresponding to a cobalt concentration of less than 2×10^{-12} mol L^{-1}. The test solutions were equilibrated in the dark over night with occasional mixing before measuring the test solution pH with an Orion 3 Star pH meter. Batch sorption experiments were done in the dark, at room temperature using constant rotary mixing (50 rpm) to equilibrate 20 mg of antimony oxide with 10 ml of the test solution (batch factor 500 mL g^{-1}). The same batch factor was used in the UV oxidation experiments, where 160 mg of antimony oxide and 80 mL of test solution were mixed in a 100 mL immersion well reactor (Photochemical Reactors Ltd., Model 3312). A quartz tube separated the 6 W low-pressure mercury lamp (major emission wavelength of 254 nm) from the reaction mixture. A bubbling system delivering compressed air through sintered glass was used to stir the reaction mixture, which was allowed to mix in the dark for 1 h before the UV-C irradiation. The temperature (22–24 °C) was controlled with a TTM-000 Series thermostat (TOHO Electronics Inc., Japan).

After mixing the suspensions, centrifugation (10 min at 3000×*g*) was used to remove the solid material from the solution. In addition, the solution was filtered with a 0.2 μm Acrodisc filter (PALL Life Sciences) to remove some very fine antimony oxide particles seen on the solution surface after centrifugation. To analyze the activity concentration of ^{57}Co in the solution, aliquots (5 ml) of the solution before and after the experiments were counted for ^{57}Co with a gamma counter (Wallac 1480 WizardTM 3). Each sample was counted for 30 min, or until a total amount of 100,000 counts had been accumulated. Considering the background count rate of approximately 20 cpm, a minimum detectable activity (MDA) of 0.08 Bq could be calculated for a typical measurement. This MDA is significantly lower than the remaining ^{57}Co activity in solution in any of the analyzed samples, allowing for the calculation of sorption distribution coefficients (K_D) for all Co-containing samples. The term K_D will be used throughout the text to describe the partitioning of cobalt between the solid and aqueous phases, independent of the type of investigation (presence or absence of EDTA and/or competing cations). In other words, the distribution coefficient was used to estimate the cobalt processing capacity (mL g^{-1}) of the antimony oxide under the prevailing conditions. The accuracy of the results was evaluated using the propagation of uncertainty.

2.5. Sorption tests without interfering ions and UV-C irradiation

The difference in the sorption efficiency between ionic cobalt and EDTA-complexed cobalt was examined in $NaNO_3$ solution with stable cobalt concentrations varying between 2 μmol L^{-1} and 10 mmol L^{-1} and EDTA concentrations varying between 0 μmol L^{-1} and 20 mmol L^{-1}. The test solution pH varied between 4.5 and 5.5. When EDTA was present in the solution, its concentration was two times higher than that of cobalt, which ensures efficient complexation of cobalt with EDTA (see Supplementary material, Table S1). The obtained sorption isotherms describe the concentration of the sorbed species in the solid phase versus its concentration in the solution at equilibrium conditions and constant temperature. Experimentally, an isotherm generally reaches a plateau, which shows the experimental sorption maximum. In order to evaluate the sorption processes, a number of isotherm equations, both theoretical and empirical, have been developed. In this study, a total number of six different isotherm models: Langmuir [13,14], Freundlich [13,14], Sips [15], Toth [16], Dubinin-Radushkevich [13] and BiLangmuir [17] (see Supplementary Material (Table S2) for detailed information) were fitted to the experimental data using the non-linear least squares method and the Levenberg-Marquardt algorithm as an optimization procedure with the Matlab Curve Fitting Tool. The tolerance values of optimization (TolX and TolFun) were set to 1×10^{-6} and the unknown parameters were estimated with 95 % confidence bounds. No weighting was used in the fitting routine.

2.6. Sorption tests with Ca^{2+} and Ni^{2+} without UV-C irradiation

To test the effect of interfering ions on the cobalt sorption of the synthesized material, 0–1000 μmol L^{-1} Ca^{2+} or Ni^{2+} was added to the $NaNO_3$ solution containing 10 μmol L^{-1} Co^{2+}. The tests were conducted in the absence and presence of 100 μmol L^{-1} EDTA. The test solution pH varied between 4.2 and 4.7.

2.7. Sorption tests with UV-C irradiation

The UV-C irradiation experiments were performed in $NaNO_3$ solution containing 10 μmol L^{-1} cobalt in the absence and presence of 100 μmol L^{-1} EDTA. The effect of interfering ions was tested adding 10 μmol L^{-1} Ca^{2+} or Ni^{2+} to the solution with 100 μmol L^{-1} EDTA.

3. Results and discussion

3.1. Antimony oxide characterization

The identification of the crystal phase of the synthesized antimony oxide was based on the X-ray diffractogram (Fig. 1, black traces, lower diffractogram) of the material. The d-spacing values with corresponding crystal planes were congruent with the diffraction data published by Abe and Itoh [18] (see Supplementary Material, Table S3) which indicates a crystal phase of $Sb_2O_5 \cdot 4H_2O$ (cubic, a: 10.3750 Å, space group *Fd3m*). The published diffraction peaks from Abe and Itoh [18] have been added to Fig. 1 for comparison (green bars). The effect of UV-C irradiation on the bulk structure of the synthesized material was also analyzed. A comparison of the diffractograms of the material before and after 24 h of UV-C irradiation in $NaNO_3$ solution containing 10 μmol L^{-1} Co^{2+} and 100 μmol L^{-1} EDTA is presented in Fig. 1 (red traces, upper diffractogram). Both diffractograms are identical, implying that UV-C irradiation has no effect on the bulk structure of the synthetic antimony oxide.

The specific surface area (BET) of the synthesized material was 49.4 m^2 g^{-1} and its porosity (total pore volume) was 0.059 cm^3 g^{-1}

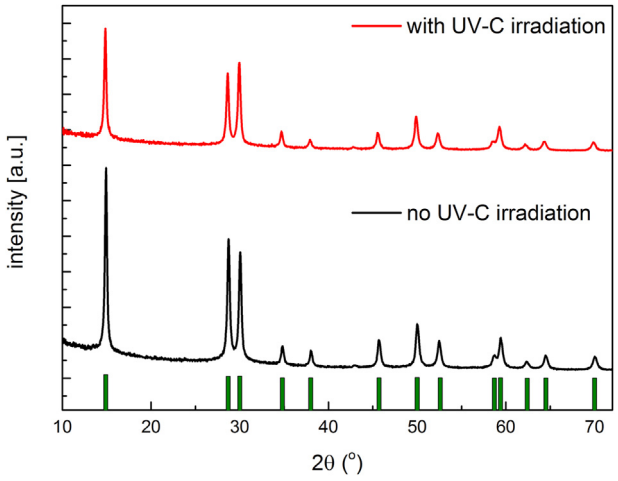

Fig. 1. The X-ray diffraction patterns of the synthesized antimony oxide before (black, lower diffractogram) and after (red, upper diffractogram) 24 h of UV-C irradiation in 0.01 M $NaNO_3$ solution containing 10 μM Co^{2+} and 100 μM EDTA. The green bars are published diffraction data for antimony oxide from Abe and Itoh [18].

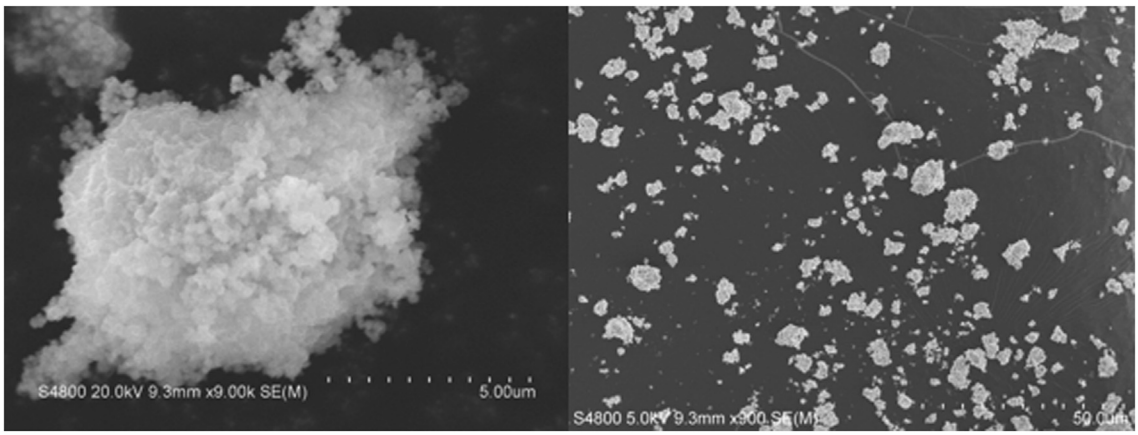

Fig. 2. FE-SEM image illustrating the particle morphology (left) and the particle size distribution (right) of the synthesized antimony oxide.

when analyzed using a dedicated transducer monitoring continuously the saturation pressure of the cryogenic bath. The FE-SEM image illustrating the morphology of the material (Fig. 2, left) reveals irregularly shaped and porous particles. The FE-SEM image with a lower magnification (Fig. 2, right) shows the wide particle size distribution of the material.

The zeta potential of the material was rather constant, −40 mV to −50 mV, between pH values 5 and 9.5, *cf.* Fig. 3. Below pH 5 the zeta potential started approaching zero and the estimation of the PZC of the material is at pH 1.4. However, due to the surface roughness, which has been shown to affect the accurate determination of the zeta potential with the micro electrophoresis method, as has been written by Delgado et al. [19], the zeta potential values of the synthesized antimony oxide shown in Fig. 3 should be used only for the estimation of the point of zero charge (PZC) of the material.

3.2. Sorption tests in the presence and absence of EDTA without interfering ions and UV-C irradiation

The batch sorption experiments in the absence and presence of EDTA were, at first, conducted in the dark to avoid any influence of UV-radiation on the Co^{2+} sorption and complexation processes. During the batch sorption experiments the test solution pH decreased from 5.5-4.5 to 3.1–2.8 as a result of cobalt uptake by the ion exchanger and the subsequent release of protons in solution. This is an indication of the acidity of the hydrous antimony oxide, $Sb_2O_5 \bullet 4H_2O$. The acidity of hydrous oxides is known to increase in the order $MO < M_2O_3 < MO_2 < M_2O_5 < MO_3$ and the higher oxides

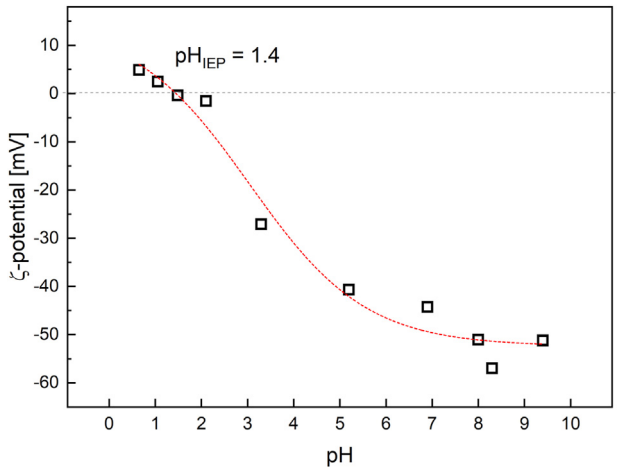

Fig. 3. The zeta potential (mV) of antimony oxide in 0.01 mol L^{-1} $NaNO_3$ solution as a function of pH after four days of constant rotary mixing at room temperature in the dark. The red dashed line has been added as a guide for the eye.

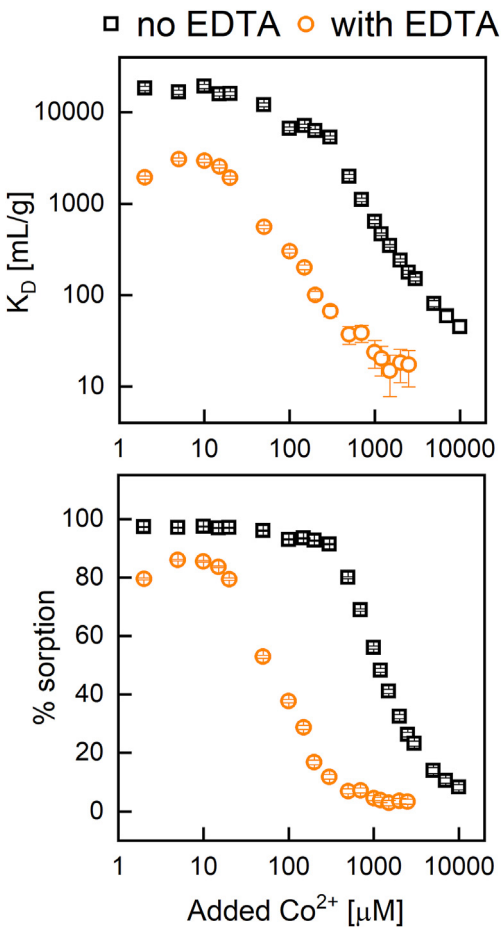

Fig. 4. ^{57}Co distribution coefficient (K_D/mL g^{-1}) (top) and ^{57}Co sorption % (bottom) on the synthetic antimony oxide in 0.01 mol L^{-1} $NaNO_3$ solution containing either Co^{2+} (black □ symbols) or Co + EDTA (orange ○ symbols), with the concentration of EDTA being two times higher than that of cobalt, after 24 h of constant rotary mixing at room temperature in the dark as a function of the initial Co^{2+} concentration (μmol L^{-1}) in the solution.

of Sb^{5+} (present in $Sb_2O_5 \cdot 4H_2O$) exhibit good cation exchange properties in acidic pH [20]. Fig. 4 presents the obtained K_D values for Co^{2+} on antimony oxide in the absence (black ▫ symbols) and presence (orange ○ symbols) of EDTA.

The discussion of the sorption data begins with the results obtained in the absence of the complexing agent. The sorption data presented in Fig. 4 (bottom) show a plateau region with almost 100% removal of Co^{2+} from solution, for added Co^{2+} concentrations up to 500 μM. Higher Co^{2+} concentrations on the other hand, lead to a decrease of the overall uptake. Based on these results, the experimental sorption capacity, q_e, of the synthesized antimony oxide was calculated and the results are presented in Fig. 5 as a function of the added Co^{2+} concentration (left) and the Co^{2+} equilibrium concentration in solution after the experiment (right).

In the isotherm data two distinct slopes can be identified (indicated in Fig. 5 with gray dashed lines). For overall Co^{2+} concentrations in the 0 to 300 μmol L^{-1} range (see dashed line in Fig. 5, left), a slope of 0.95 ± 0.09 can be discerned for cobalt concentrations below 50 μmol L^{-1}, which decreases slightly to 0.89 ± 0.08 when considering total Co^{2+} concentrations up to 300 μmol L^{-1}. In this concentration range, the sorption reaction is independent of the total metal ion concentration used, resulting in a linear uptake behavior, referred to as the ideal sorption range. Above Co^{2+} concentrations of 300 μmol L^{-1}, the slope decreases significantly to 0.22 ± 0.03, indicative of Co^{2+} uptake outside the ideal sorption range. The reason for ideal vs. non-ideal sorption behavior can be attributed to e.g. the presence of different site types on the antimony oxide, responsible for metal ion uptake in the different concentration regimes. At low concentrations so called strong site types are assumed to participate in the sorption reaction, while weak site types become active when the total metal ion concentration increases and the amount of strong site types becomes saturated. However, surface saturation and steric effects may also contribute to non-linear sorption behavior.

Abe [21] and Baetsle and Huys [22] have calculated the theoretical exchange capacity of $Sb_2O_5 \bullet 4H_2O$ as 5.06 meq g^{-1} which in the case of Co^{2+} corresponds to 2.5 mmol g^{-1}. According to Abe and Sudoh [23], however, the maximum uptake of Co^{2+} by crystalline antimony oxide in 0.1 mol L^{-1} cobalt nitrate solution was found to be 0.61 meq g^{-1} corresponding to 0.3 mmol g^{-1}. In their study, the ion exchange equilibrium for 20 mg of solid material and 20 mL of solution was attained after 10 days. As can be seen in Fig. 5, the Co^{2+} uptake of the synthesized antimony oxide was in the same order of magnitude, 0.41 mmol g^{-1}, in $NaNO_3$ solution containing 10 mmol L^{-1} cobalt. The low exchange capacity in comparison to the theoretical one, may arise from the strong hydration of small cations such as Co^{2+}, Ni^{2+} and Zn^{2+} (effective ionic radii being 0.745, 0.69 and 0.74 Å, respectively for coordination number VI [24]) in aqueous solution. It is possible that the hydration volumes of the cations contribute more to the steric effect than the crystal ionic radii. Thus, the theoretical exchange capacity may not be reached.

When EDTA was added to the antimony oxide suspensions, the uptake of Co^{2+} by the synthesized material decreased significantly in comparison to the suspension without EDTA (Figs. 4 and 5). Based on the calculated Co-EDTA solution speciation (Table S1) using the chemical speciation program Visual Minteq (version 3.0) [25] and stability constants for $CoEDTA^{2-}$, CoHEDTA and CoH_2EDTA of 18.16, 21.59 and 23.49, respectively [26,27] less than 5 % of cobalt should remain uncomplexed by the EDTA ligand under all experimental conditions.

When plotting the sorption percentages of Co^{2+} on antimony oxide in the "plateau"-area where more than 96% of the added Co^{2+} is retained on the ion exchanger in the absence of EDTA together with the corresponding data in the presence of EDTA, the influence of the complexing agent can be seen to be considerable (Fig. 4, bottom). This emphasizes the importance of decomplexation of radioactive contaminants from strong ligands such as EDTA, before commencing with purification of the solutions with ion exchangers and other solid phases.

The batch sorption data in the presence of EDTA seems to reach a sorption plateau around 5 % for Co^{2+} concentrations above 500 μM (Fig. 4, bottom). Based on our speciation modeling, all cobalt should be complexed by the EDTA ligand in this concentration

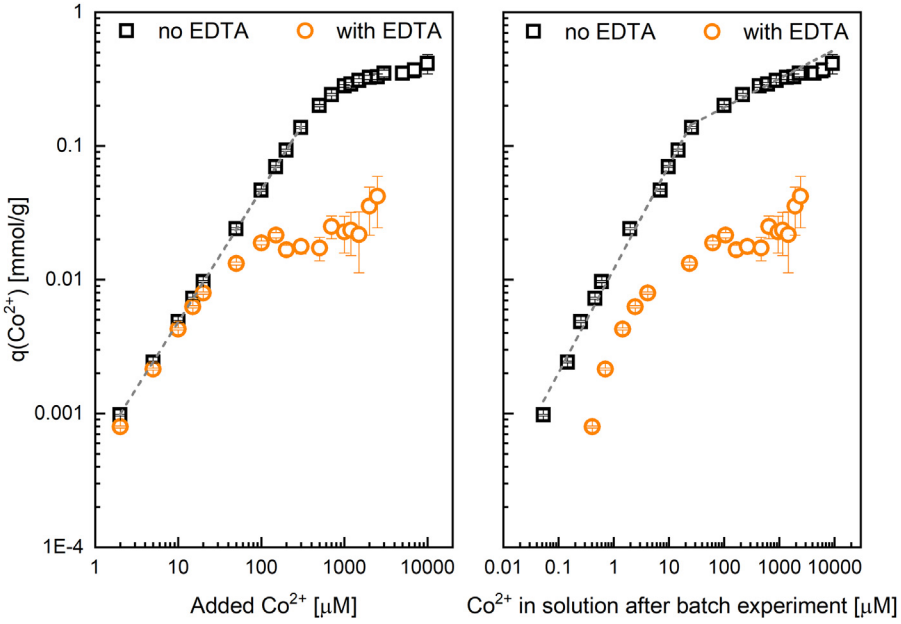

Fig. 5. The uptake of Co^{2+}, q_e (mmol g^{-1}) as a function of added Co^{2+} (left) and the equilibrium Co^{2+} concentration in solution after the experiment (right), after 24 h of constant rotary mixing at room temperature in the dark with the synthesized antimony oxide, in 0.01 mol L^{-1} $NaNO_3$ solution containing varying amounts of Co^{2+} (black ◻ symbols) or the Co-EDTA complex (orange ○ symbols), with the concentration of EDTA being two times higher than that of cobalt, as a function of the Co^{2+} concentration (μmol L^{-1}) in the solution.

range, which implies that some additional reactions take place in the antimony oxide suspensions. It is possible that a small amount of the neutral CoH_2EDTA complex adsorbs on the ion exchange material. The calculated amount of CoH_2EDTA in solution in the Co^{2+}-concentration range above 500 μM is between 4 and 10%, which matches very well with the sorption plateau observed in our batch sorption studies. Other possibilities for the small amount of sorption taking place at these rather high Co^{2+} and EDTA concentrations is the presence of non-complexed Co^{2+} due to e.g. competing complexation reactions with Sb and the complexing ligand. The excess EDTA in solution can promote the dissolution of Sb from the antimony oxide and further enable the formation of Sb-EDTA complexes. Since the amount of antimony in the solution was not analyzed in the present study it is not possible to estimate the effect of EDTA on the synthesized antimony oxide. Thus, this solid/solution system should be considered as a multiple ligand system where EDTA and the surface of the antimony oxide compete for cationic cobalt.

Finally, to examine the obtained experimental sorption data further, six different isotherm models were fitted to the experimental data. The Langmuir isotherm assumes that sorption takes place at specific homogenous sites of the sorbent without any mutual interactions between the sorbates. The Freundlich isotherm is applicable for heterogeneous surfaces. The Sips isotherm is a combination of the Langmuir and Freundlich isotherms and takes into account the surface heterogeneity. The Toth model is an empirical equation, derived to improve the Langmuir model applicability at both low and high concentration limits and it is suitable in modeling of heterogeneous sorption processes. The Dubinin-Radushkevich isotherm assumes a Gaussian energy distribution and includes the effect of temperature and it can be used to evaluate the sorption energies. Finally, the BiLangmuir isotherm containing four parameters presumes that the sorbent surface has two Langmuir-like active sites with different affinities towards the target sorbing species. The results of the isotherm modeling are presented in Table 1.

For the solution containing only Co^{2+}, the best fit was obtained with the Sips, Toth and BiLangmuir models. From these models the Sips model estimated the experimental sorption maximum with the highest accuracy and therefore can be assigned to be the most suitable among the tested models (Fig. 6). It is also one of the best models to describe the sorption of Co^{2+} in the presence of EDTA.

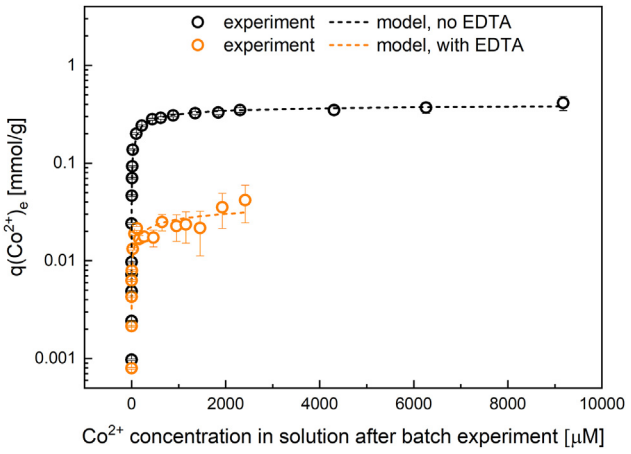

Fig. 6. Fitting the Sips isotherm model (dashed line) to the experimental values of the uptake of Co^{2+}, q_e (mmol g^{-1}) on the synthesized antimony oxide in the absence (black □ symbols) and presence (orange ○ symbols) of EDTA, in 0.01 mol L^{-1} $NaNO_3$ solution as a function of the Co^{2+} concentration (μmol L^{-1}) in the solution after 24 h of constant rotary mixing at room temperature in the dark. The EDTA concentration in the experiments was two times higher than that of cobalt.

The good fit of the Sips model indicates that the synthesized antimony oxide is a heterogeneous sorbent material, with different types of sorption sites. In the model the n_S value describes the surface heterogeneity. When the n_S value deviates from unity, it denotes heterogeneous adsorbent surface. On the other hand, when the n_S value equals unity, the Sips isotherm returns to the Langmuir isotherm and indicates homogeneous adsorption [28]. Thus, the heterogeneity of the material was also verified by the n_S value of 0.592 which is clearly less than unity. The modeling results corroborate the isotherm data presented in Fig. 5 left, where two sorption regimes, ideal and non-ideal ones, could be identified.

Based on the correlation coefficients (R^2) and comparison of the calculated maximum sorption (q_m) to the experimental maximum sorption value determined for antimony oxide ($q_{m,exp}$) (Table 1), fitting was seen to be poor in the case of the solution containing both Co^{2+} and EDTA. This can be attributed to the low sorption efficiency since the removal of cobalt in the presence of EDTA decreased from 79.5 % to 3.3 % when the concentration of cobalt

Table 1
Sorption isotherm parameters for Co^{2+} sorption of antimony oxide observed from fitting the experimental sorption data from Fig. 5 with six isotherm models. Parameters were obtained with 95 % confidence bounds. R^2 refers to the correlation coefficient and χ^2/ν is chi-squared per degree of freedom.

Langmuir		$q_{m,exp}$ (mmol/g)	q_{mL} (mmol/g)	K_L (l/mmol)			R^2	χ^2/ν
	Co	0.413	0.350	16.1			0.976	0.0045
	Co-EDTA	0.042	0.025	33.6			0.707	0.0017
Freundlich		$q_{m,exp}$ (mmol/g)		K_F (l/mmol)	n_F		R^2	
	Co	0.413		0.275	4.50		0.938	0.1605
	Co-EDTA	0.042		0.027	4.03		0.851	0.0018
Sips		$q_{m,exp}$ (mmol/g)	q_{mS} (mmol/g)	K_S (l/mmol)	n_S		R^2	
	Co	0.413	0.410	7.94	0.592		0.994	0.0039
	Co-EDTA	0.042	0.063	0.410	0.335		0.916	0.0015
Toth		$q_{m,exp}$ (mmol/g)	q_{mT} (mmol/g)	b_T (l/mmol)	n_T		R^2	
	Co	0.413	0.443	0.157	0.426		0.996	0.0010
	Co-EDTA	0.042	0.263	1.19	0.338		0.889	0.0045
Dubinin-Radushkevich		$q_{m,exp}$ (mmol/g)	q_{mRP} (mmol/g)	b_{DR}	E (kJ/mol)		R^2	
	Co	0.413	0.343	0.080	6.15		0.978	0.0031
	Co-EDTA	0.042	0.027	0.049	7.80		0.755	0.0019
BiLangmuir		$q_{m,exp}$ (mmol/g)	q_{mBL1} (mmol/g)	K_{BL1} (l/mmol)	q_{mBL2} (mmol/g)	K_{BL2} (l/mmol)	R^2	
	Co	0.413	0.262	36.1	0.163	0.454	0.997	0.0009
	Co-EDTA	0.042	0.021	20.1	0.172	0.036	0.926	0.0049

increased from 2 μmol L^{-1} to 2500 μmol L^{-1} (the concentration of EDTA being two times higher than that of cobalt). The experimental sorption data scattered to some extent in the presence of EDTA as can be seen in Fig. 6 depicting the Sips isotherm for cobalt uptake values from Fig. 5. The maximum sorption was estimated as 0.063 mmol g^{-1} by the Sips model and was the best estimation of the obtained experimental value, 0.042 mmol g^{-1}. The other models estimated the experimental cobalt uptake as 0.021–0.0265 mmol g^{-1} or 0.263 mmol g^{-1} as can be seen from Table 1.

Based on theory, energy values (E) from the Dubinin-Radushkevich model can be used to evaluate the sorption mechanism. E values less than 8 kJ mol^{-1} indicate physical sorption and values from 8 to 16 kJ mol^{-1} support ion exchange [29,30]. For the solution containing only cobalt, the E value was 6.2 kJ mol^{-1} and for the solution containing the Co-EDTA complex, the E value was 7.8 kJ mol^{-1}. The E values indicate that the removal of Co^{2+} could be attributed to physical sorption. However, e.g. Inglezakis and Zorpas [31] revealed in their research that adsorption energy values as low as 0.6 kJ mol^{-1} were obtained for ion exchange on zeolite clinoptilolite using the Dubinin-Radushkevich model. They collected a large number of experimental adsorption energy values from the literature, of which 38 % were derived by the use of the Dubinin-Radushkevich model. The maximum values obtained were very close to the proposed range of ion exchange (<16 kJ mol^{-1}) but the lower limit was not accurate. Taking into account, that the correlation coefficients for the Dubinin-Radushkevich model were 0.978 and 0.755 (Table 1), extra care should be taken when interpreting the results.

Based on the results presented in Fig. 5, also the selectivity coefficient $K_{Co/H}$ was calculated and is presented as a function of the experimental cobalt uptake, q_e, in Fig. 7. As the cobalt concentration increases, the selectivity coefficient decreases which is a rather well-known phenomenon with selective ion exchange materials. The counter ion with higher valence is preferred and the preference increases with dilution of the solution. Selectivity of the synthesized antimony oxide is strongly reduced in the presence of EDTA.

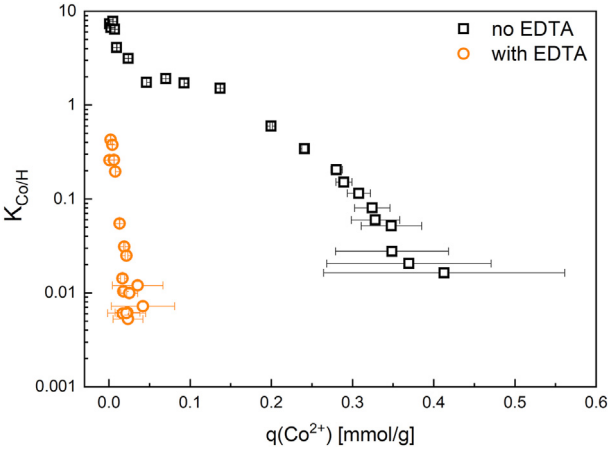

Fig. 7. The selectivity coefficient ($K_{Co/H}$), in 0.01 mol L^{-1} $NaNO_3$ solution containing varying amounts of Co^{2+} (black □ symbols) or the Co-EDTA complex (orange ○ symbols), with the concentration of EDTA being two times higher than that of cobalt, as a function of the experimental cobalt sorption capacity (mmol g^{-1}) of the synthesized antimony oxide after 24 h of constant rotary mixing at room temperature in the dark.

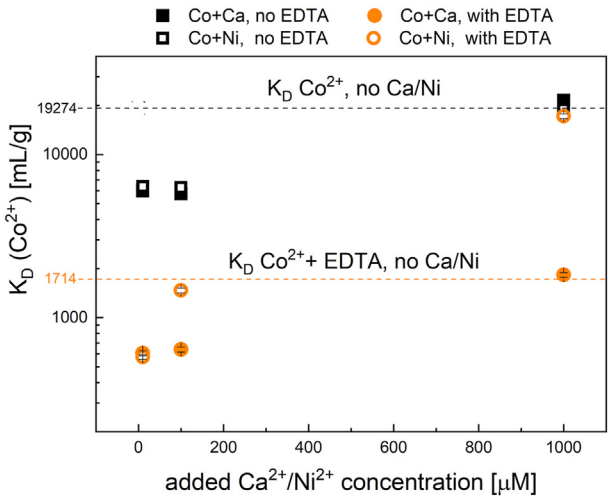

Fig. 8. Sorption distribution coefficients (K_D) of 10 μM Co^{2+} in 0.01 mol L^{-1} $NaNO_3$ solution as a function of Ca^{2+} (closed symbols) or Ni^{2+} (open symbols) concentration in the absence (black, □) and presence (orange, ○) of EDTA after 24 h of constant rotary mixing at room temperature in the dark. The vertical lines indicate the K_D values of 10 μM Co^{2+} in the absence of competing metals.

3.3. Sorption competition investigations with Ca^{2+} and Ni^{2+} in the absence of UV-C irradiation

3.3.1. Influence of Ca^{2+} and Ni^{2+}

The selectivity of antimony oxide towards Co^{2+} and Ca^{2+} has not been published, while some literature on Co^{2+} vs. Ni^{2+} uptake can be found. According to Abe and Kasai [32], crystalline antimony oxide is more selective towards Co^{2+} than Ni^{2+} in nitric acid solutions containing 100 μM metal ions. In our sorption investigations we wanted to study the selectivity between Co^{2+} and Ca^{2+} or Ni^{2+}. The results are presented in Fig. 8 for three competing metal concentrations of 10 μM, 100 μM, and 1000 μM. It can be seen that the uptake of Co^{2+} on antimony oxide decreases by a factor of more than 3 in the presence of 10–100 μM Ca^{2+} or Ni^{2+} (Fig. 8). Here, the total metal ion concentration is still within the ideal sorption range as discussed above in connection to the Co^{2+} sorption experiments presented in Fig. 5. The "strong" sorption sites which are active in this sorption range must, thus, be responsible for the selectivity of Ca^{2+} and Ni^{2+} over Co^{2+}. As the competing metal ion concentration in the solution increases, the preference towards cobalt increases. This can be seen for Co^{2+} uptake in the presence of 1000 μM Ca^{2+} or Ni^{2+} where the obtained K_D value for Co^{2+} is almost identical to the sorption distribution coefficient obtained in the absence of any competing metals (indicated in Fig. 8 with a dashed line). In these experiments, the sorption occurs in the non-ideal sorption range where "weak"-sites are responsible for the uptake of metal ions from solution. These weak sites seem to have no preference for calcium or nickel over cobalt, but rather Co^{2+} uptake is promoted in this concentration range. No clear difference between the competing metals can be seen, i.e. both Ca^{2+} and Ni^{2+} seem to influence the uptake of Co^{2+} by the ion exchanger in a very similar fashion. Thus, the selectivity of the ion exchanger toward Co^{2+} is determined by the overall metal ion concentration in solution.

When considering a typical NPP floor drain water effluent, Ca^{2+} accounts for the majority of the divalent metal ion concentration in the waste solution while the activation products Ni and Co are present in trace concentrations only. With an overall Ca^{2+} concentration in the millimolar concentration range [10], cobalt removal from the waste solution using antimony oxide should not be hampered according to the results obtained in our sorption

investigations. This, however, applies only for waste solutions that do not contain EDTA. The influence of EDTA on the specific sorption of Co, Ni, and Ca on antimony oxide will be discussed below.

3.3.2. *Influence of Ca^{2+} and Ni^{2+} in the presence of EDTA*

In the presence of both Ca^{2+} and EDTA, the Co^{2+} sorption distribution coefficient is even lower than in the presence on EDTA only. This can be explained by the much smaller Ca^{2+}-EDTA stability constants in comparison to the Co^{2+}-EDTA ones, see Table S4. According to the calculation with the chemical speciation program Visual Minteq (version 3.0), using the M^{2+}-EDTA stability constants given in the Supplementary material (Table S4), calcium is in free ionic form below pH 3.5 and only cobalt forms complexes with EDTA [26]. The free Ca^{2+} can adsorb on the ion exchange material, further blocking sorption sites on the solid surface, resulting in a lower cobalt K_D value in the presence of calcium as presented in Fig. 8. Similar to our observations in the absence of EDTA, the selectivity towards cobalt in the EDTA bearing solution increases with increasing calcium concentration and the sorption distribution coefficient in 1000 μmol L^{-1} Ca^{2+} solution becomes identical to the K_D value obtained in the complete absence of Ca^{2+} (value indicated by vertical orange line in Fig. 8). Thus, the overall uptake of cobalt at these high Ca^{2+} concentrations is only influenced by EDTA and the formation of soluble Co-EDTA complexes in solution.

In the presence of Ni^{2+}, only the lowest concentration of 10 μM decreases the Co^{2+} uptake in a similar manner as noted for Ca^{2+}. A further increase of Ni^{2+} to 100 μM almost completely removes the influence of the competing metal cation, resulting in a Co^{2+} K_D value close to the one obtained in the absence of Ni^{2+}. This can be understood when considering the relative stabilities of the divalent metal ion complexes with EDTA (Table S4).

3.4. *Sorption tests with UV-C irradiation*

To investigate the influence of UV-C irradiation on Co^{2+} uptake by the potentially photocatalytic antimony oxide and the possible photodegradation of EDTA, sorption investigations were conducted in the absence and presence of EDTA and the competing cations Ca^{2+} and Ni^{2+} under UV-C irradiation. The results are summarized in Fig. 9.

Interestingly, the K_D value in the solution containing only ionic cobalt is significantly increased due to UV-C irradiation. This must be related to a change in the cobalt speciation, most likely the oxidation of Co^{2+} to Co^{3+}, either due to the photocatalytic activity of the synthetic antimony oxide or the formation of solution radicals by the external light source. The photocatalytic activity of hydrous antimony oxides for the oxidation of benzene has been studied recently by Chen et al. [33]. In their study, hydrous antimony oxides were synthesized with some variations and the highest photocatalytic activity was reached with a material with the highest BET surface area (38.2 m^2 g^{-1}). They concluded that the large amount of $O_2^{\bullet-}$ and long lived $^{\bullet}OH$ over hydrous antimony oxide under UV-C irradiation was the main reason for the good photocatalytic activity and for the obtained mineralization rates of benzene which were higher than those of TiO_2 P25, a standard material used to achieve photocatalytic reactions. The BET surface area of the synthesized antimony oxide presented in this study is 49.4 m^2 g^{-1} implying high photocatalytic activity for Co^{2+} oxidation.

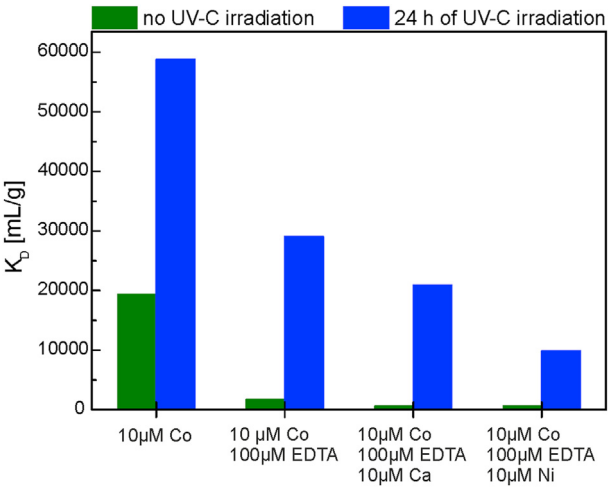

Fig. 9. Sorption distribution coefficients (K_D) of the test solutions in the absence and presence of EDTA without (green column, left) and with (blue column, right) 24 h of UV-C irradiation.

One of the articles reporting the oxidation of Co^{2+} to Co^{3+} under UV irradiation is written by Rekab et al. [9]. In their research an UV source with photonic power of 17 W (254 nm) was used to irradiate Co-EDTA solutions for 3 h. The oxidation did not involve reduction of nitrates, since identical results were obtained with $CoCl_2$, thus the oxidation was caused only by the UV-C irradiation. Eaton and Suart [34] have proposed the following equation for the oxidation of Co^{2+} by water, Eq. (1):

$$Co^{2+} + H_2O \rightarrow Co^{3+} + OH^- + \tfrac{1}{2}\,H_2 \quad (1)$$

In our research a 6 W UV source was used but even though the photonic power is lower than in the study of Rekab et al. [9], the possibility of Co^{2+} oxidation to Co^{3+} should be taken into account. For example, the log K for the Co^{3+}-EDTA complex is over 40, which is considerably larger than the stability of Co^{2+}-EDTA (Table S4). After UV-C irradiation of the antimony oxide suspension containing both cobalt and EDTA, an increase of the K_D value can again be seen in comparison to the non-irradiated EDTA-containing solution. The K_D value after UV-C irradiation is higher than the K_D value obtained in the solution containing only ionic cobalt that has not been exposed to light but smaller than the K_D obtained for ionic cobalt under UV-C irradiation. This implies that degradation of EDTA has occurred in combination with cobalt oxidation, however, either the oxidation has not progressed to the same extent as observed in the EDTA-free solution or some of the EDTA has not been photodegraded but remains complexed to cobalt, keeping it in solution.

In the 10 μM calcium bearing Co-EDTA solution, the K_D value after UV-C irradiation is slightly higher than for Co^{2+} in the absence of any competing cations or ligands but much lower than observed in the presumed oxidation of Co^{2+} to Co^{3+} after UV-C treatment. This implies that the oxidation reaction happens at the antimony oxide surface and not in solution. As the sorption of Co^{2+} is strongly reduced by the introduction of Ca^{2+} (and Ni^{2+}, which will be discussed later), a much lower amount of cobalt is consequently oxidized. Calcium cannot be oxidized to a higher oxidation state in aqueous solution, which indicates that the obtained K_D value under UV-C irradiation must be explained by partial oxidation of cobalt and degradation of the EDTA complex under UV-C irradiation. If the EDTA complex would not be degraded, the higher stability of Co^{3+}-EDTA compared to the stability of Co^{2+}-EDTA would have resulted in the formation of a strong Co-EDTA complex subsequently decreasing the uptake of Co^{3+} on the antimony surface resulting in a lower K_D value.

When examining the results obtained using the nickel bearing Co-EDTA solution, it can be seen that the K_D value obtained under UV-C irradiation is much lower than in the Co-EDTA solution with and without calcium. As both Ni^{2+} and Ca^{2+} were shown to have a

similar influence on the uptake of Co^{2+} at concentrations of 10 μM, both in the presence and absence of EDTA (see Fig. 8), the nickel system must include additional reactions after UV-C treatment which are absent in the calcium one. These must be related to the redox behavior of nickel and the production of other oxidation states than Ni^{2+}, which are capable of suppressing the sorption of Co^{2+} on the surface and the subsequent oxidation of Co^{2+} to Co^{3+}. One possibility is the oxidation of Ni^{2+} to Ni^{3+}, which could influence the amount of cobalt sorption on the solid surface. Such Ni^{2+} oxidation has been described on the hematite surface after photoexcitation of hematite (α-Fe_2O_3) by Wang et al. [35]. It is clear that any free, non-complexed (i.e. surface sorbed or EDTA associated) Co^{3+}/Ni^{3+} is expected to undergo immediate reduction to Co^{2+} and Ni^{2+} after the UV-treatment when considering the stability fields of the various species in aqueous solution [9,36]. As a detailed description of the redox chemistry of Co/Ni is not the scope of the present paper, we can only conclude that UV-C irradiation enhances the selectivity between Co and Ni but that nickel clearly interferes with the removal of cobalt, even after UV-C treatment which should enhance cobalt uptake as a consequence of photocatalytic oxidation of Co^{2+} to Co^{3+} at the antimony oxide surface. As nickel is one of the activation corrosion products in the NPP waste effluents and needs to be removed e.g. by ion exchange, the low selectivity difference between Co and Ni could, in some cases, be considered as benefit if both metals should be removed from the liquid waste.

Taking into account the effect of UV-C irradiation, not only to the EDTA bearing solution, but also to the solution containing ionic cobalt, UV-C irradiation can be considered as an efficient addition for the Co^{2+} sorption process with antimony oxide. Particulate cobalt can be removed from the NPP effluents by filtration but the soluble forms of cobalt require the use of e.g. precipitation or ion exchange. Precipitation produces a rather difficult waste form, radioactive sludge, which usually requires solidification in e.g. cement and contains also inactive metals which were present in the effluent. Using selective ion exchange results in a smaller amount of solid waste as the accumulation of inactive metals is avoided and only the target radionuclide is removed from the effluent. Since the synthesized antimony oxide did not show high selectivity between Co and Ca or Ni in the equimolar solutions in the dark, it was interesting to find out that UV-C irradiation enhanced the K_D values when equimolar amounts of Co and Ca or Ni were present in the solution. However, the K_D values in the presence of Ca or Ni are still lower than the values obtained without the interfering ions indicating that these ions can interfere with the sorption of cobalt on the synthesized antimony oxide.

4. Conclusions

The heterogeneity of the synthesized antimony oxide was demonstrated by the batch sorption experiments and further reasoned by the Sips model, which fitted the experimental data with the highest accuracy from the six different sorption isotherm models used. The characteristics of the involved metals; cobalt, calcium and nickel, and their competition for adsorption sites on the adsorbent, the presence of EDTA and adsorbent characteristics were shown to have an effect on the cobalt adsorption.

The effect of UV-C irradiation on the cobalt sorption efficiency of the synthesized antimony oxide was emphasized in this study. Based on the results obtained from the UV-C irradiation experiments, it was concluded that the possible oxidation of cobalt and degradation of the EDTA complex enhanced the cobalt sorption efficiency also in the presence of interfering ions, calcium or nickel. No additional oxidizer, such as e.g. H_2O_2, was used in the experiments. This can be considered highly beneficial since the addition of each chemical in the treatment system complicates the system to some extent.

In the presence of millimolar concentrations of calcium, the removal of cobalt by the synthesized antimony oxide should not be hindered. Nickel, being chemically similar with cobalt, affected the sorption of cobalt more than calcium in the UV-C irradiation experiments. If simultaneous sorption of cobalt and nickel could be done efficiently with the synthesized antimony oxide, it could be considered beneficial. However, the possible simultaneous cobalt and nickel adsorption capability of the antimony oxide should be studied further. In order to fully understand the sorption behavior and possible oxidation of the solution components, the concentration of calcium, nickel and EDTA in the solution should be analyzed in future studies and combined with investigations regarding the redox chemistry of the involved elements.

According to the XRD analysis, the bulk structure of the synthesized antimony oxide showed no changes during UV-C irradiation, which emphasized the usability of the material in liquid waste treatment systems utilizing UV-C irradiation.

Declaration of competing interest

The authors declare that they have no known competing financial interests or personal relationships that could have appeared to influence the work reported in this paper.

Acknowledgements

This work was supported by the Jenny and Antti Wihuri Foundation [2015] and the Fortum Foundation [201500073, 2016]. Anna-Elina Pasi, M. Sc. and Taneli Iso-Markku, M. Sc., are thanked for the assistance with the laboratory experiments. Liisa Puro, Ph.D., is thanked for the surface area and pore size analysis. Prof. Jukka Lehto is thanked for constructive discussions throughout the course of the project.

Appendix A. Supplementary data

Supplementary data to this article can be found online at https://doi.org/10.1016/j.net.2021.08.002.

References

[1] The Lund/LBNL nuclear data search, 28th April, 2019, www.nucleardata.nuclear.lu.se/toi/.
[2] W.D. Samuels, D.M. Camaioni, H. Babad, Initial laboratory studies into the chemical and radiological aging of organic materials in underground storage tanks at the Hanford Complex. In: Proceedings of Waste Management'94: Working towards a Cleaner Environment, Tucson, AZ, United States, 27 Feb - 3 Mar 1994.
[3] J.S. Fritz, G.H. Schenk, in: Quantitative Analytical Chemistry, fifth ed., Prentice Hall, New Jersey, USA, 1987.
[4] H.G. Langer, Solid complexes with tetravalent metal ions and ethylenediamine tetra-acetic acid (EDTA), J. Inorg. Nucl. Chem. 26 (1964) 59–72.
[5] F.G. Kari, W. Giger, Modeling the photochemical degradation of ethylenediaminetetraacetate in the River Glatt, Environ. Sci. Technol. 29 (1995) 2814–2827.
[6] S. Metsärinne, T. Tuhkanen, R. Aksela, Photodegradation of ethylenediaminetetraacetic acid (EDTA) and ethylenediamine disuccinic acid (EDDS) within natural UV radiation range, Chemosphere 45 (2001) 949–955.
[7] H.B. Lockhart, R.V. Blakeley, Aerobic photodegradation of Fe(III)-(ethylenedinitrilo)tetraacetate (ferric EDTA), Environ. Sci. Technol. 9 (1975) 1035–1038.
[8] L.K. Malinen, R. Koivula, R. Harjula, Removal of radiocobalt from EDTA-complexes using oxidation and selective ion exchange, Water Sci. Technol. 60 (2009) 1097–1101.
[9] K. Rekab, C. Lepeytre, F. Goettmann, M. Dunand, C. Guillard, J.-M. Herrmann, Degradation of a cobalt(II)-EDTA complex by photocatalysis and H2O2/UV-C, Application to nuclear wastes containing ^{60}Co, J. Radioanal. Nucl. Chem. 303 (2015) 131–137.
[10] R. Harjula, J. Lehto, A. Paajanen, L. Brodkin, E. Tusa, Testing of highly selective CoTreat ion exchange media for the removal of radiocobalt and other activated corrosion product nuclides from NPP waste waters. In: Proceedings of

Waste Management, Tucson, AZ, United States, 28 Feb - 4 Mar 1999.
[11] L. Malinen, R. Koivula, R. Harjula, Removal of cobalt from aqueous solution containing EDTA under UV-C irradiation by antimony oxide, Radiochim. Acta 104 (6) (2016) 415–422.
[12] A.A. Khan, M.M. Alam, New and novel organic-inorganic type crystalline polypyrrolel/polyantimonic acid' composite system: preparation, characterization and analytical applications as a cation-exchange material and Hg(II) ion-selective membrane electrode, An. Chim. Acta 504 (2004) 253–264.
[13] K.Y. Foo, B.H. Hameed, Insights into the modeling of adsorption isotherms systems, Chem. Eng. J. 150 (1) (2010) 2–10.
[14] S.J. Allen, G. McKay, J.F. Porter, Adsorption isotherm model for basic dye adsorption by peat in single and binary component systems, J. Colloid Interface Sci. 280 (2) (2004) 322–333.
[15] A.B. Pérez-Marín, V. Meseguer Zapata, J.F. Ortuño, M. Aguilar, J. Saéz, M. Lloréns, Removal of cadmium from aqueous solutions by adsorption onto orange waste, J. Hazard Mater. 139 (1) (2007) 122–131.
[16] K. Vijayraghavan, T.V.N. Padmesh, K. Palanivelu, M. Velan, Biosorption of nickel(II) ions onto Sargassum wightii: application of two-parameter and three-parameter isotherm models, J. Hazard Mater. 133 (1) (2006) 304–308.
[17] K.G. Karthikeyan, M.A. Tshabalala, D. Wang, M. Kalbasi, Solution chemistry effects on orthophosphate adsorption by cationized wood residues, Environ. Sci. Technol. 38 (2004) 904–911.
[18] M. Abe, T. Itoh, Synthetic inorganic ion exchange materials XXV. Change in the ion-exchange selectivity by thermal treatment of crystalline antimonic(V) acid toward alkali metal ions, J. Inorg. Nucl. Chem. 42 (1980) 1641–1644.
[19] A.V. Delgado, F. González-Caballero, R.J. Hunter, L.K. Koopal, J. Lyklema, Measurement and interpretation of electrokinetic phenomena, Pure Appl. Chem. 77 (10) (2005) 1753–1805.
[20] M. Abe, Oxides and hydrous oxides of multivalent metals as inorganic ion exchangers, in: A. Clearfield A (Ed.), Inorganic Ion Exchange Materials, first ed., CRC Press, Florida, 1982, pp. 161–246.
[21] M. Abe, Ion exchange selectivities of crystalline antimonic acid, in: P.A. Williams, M.J. Hudson (Eds.), Recent Developments of Ion Exchange: Proceedings of the International Conference on Ion Exchange Processes (ION-EX '87): the North East Wales Institute of Higher Education, Elsevier Applied Science, UK, London and New York, 1987, pp. 277–290.
[22] L.H. Baetsle, D. Huys, Structure and ion exchange characteristics of poly-antimonic acid, J. Inorg. Nucl. Chem. 30 (1968) 639–649.
[23] M. Abe, K. Sudoh, Synthetic inorganic ion-exchange materials. XXIII. Ion-exchange equilibria of transition metals and hydrogen ions on crystalline antimonic(V) acid, J. Inorg. Nucl. Chem. 42 (1980) 1051–1055.
[24] R.D. Shannon, C.T. Prewitt, Effective ionic radii in oxides and fluorides, Acta Crystallogr. B25 (1969) 925–946.
[25] J.P. Gustafsson, Visual Minteq 3.0, a free equilibrium speciation model, accessed 28th April, 2019), http://vminteq.lwr.kth.se/.
[26] A.E. Martell, R.M. Smith, Critical Stability Constants, 3, Plenum, New York, 1977.
[27] J.M. Zachara, S. Smith, J.K. Fredrickson, The effect of biogenic Fe(II) on the stability and sorption of Co(II)EDTA^{2-} to goethite and a subsurface sediment, Geochem. Cosmochim. Acta 64 (8) (2000) 1345–1362.
[28] D.G. Kinniburgh, General purpose adsorption isotherms, Environ. Sci. Technol. 20 (1986) 895–904.
[29] B.S. Krishna, D.S.R. Murty, B.S. Prakash Jai, Thermodynamics of chromium(VI) anionic species sorption onto surfactant-modified montmorillonite clay, J. Colloid Interface Sci. 229 (2000) 230–236.
[30] M.E. Argun, S. Dursun, C. Ozdemir, M. Karatas, Heavy metal adsorption by modified oak sawdust: thermodynamics and kinetics, J. Hazard Mater. 141 (2007) 77–85.
[31] V.J. Inglezakis, A.A. Zorpas, Heat of adsorption, adsorption energy and activation energy in adsorption and ion exchange systems, Desal. Water Treat. 39 (2012) 149–157.
[32] M. Abe, K. Kasai, Synthetic inorganic ion-exchange materials. XXII. Distribution coefficients and possible separation of transition metals on crystalline antimonic(V) acid as a cation exchanger, Separ. Sci. Technol. 14 (1979) 895–907.
[33] J. Chen, Z. Chen, X. Zhang, X. Li, L. Yu, D. Li, Antimony oxide hydrate (Sb2O5·3H2O) as a simple and high efficient photocatalyst for oxidation of benzene, Appl. Catal. B Environ. 210 (2017) 379–385.
[34] D.R. Eaton, S.R. Suart, Electron spin resonance studies of the photooxidation and reduction of cobalt complexes, J. Phys. Chem. 72 (2) (1968) 400–405.
[35] G. Wang, Y. Ling, X. Lu, T. Zhai, F. Qian, Y. Tong, Y. Li, A mechanistic study into the catalytic effect of Ni(OH)2 on hematite for photoelectrochemical water oxidation, Nanoscale 5 (2013) 4129–4133.
[36] B. Beverskog, I. Puigdomenech, Revised Pourbaix diagrams for nickel at 25-300ºC, Corrosion Sci. 39 (1997) 969–980.